Aerosol Science and Technology

ISSN: 0278-6826 (Print) 1521-7388 (Online) Journal homepage: www.tandfonline.com/journals/uast20

Laboratory-based calibration procedure for filter-based absorption photometers using photothermal interferometry and the extinction-minus-scattering method

Tobias Hammer , Luka Drinovec , Griša Močnik , Asta Gregorič , Martin Rigler , Thomas Müller , Sebastian Düsing , Jorge Saturno, Andreas Nowak, John Backman , Eija Asmi , Krzysztof Ciupek , Douglas Walker , Maria Gini , Konstantinos Eleftheriadis , Stergios Vratolis , Jeffrey Blair , Ivan Iskra , Kyan Shlipak , Weidong Chen , Goufrane Abichou , Yongyong Hu , Jošt V. Lavrič, Johannes Murg , Michael Arndt , Alejandro Keller , Ernest Weingartner & Konstantina Vasilatou

To cite this article: Tobias Hammer , Luka Drinovec , Griša Močnik , Asta Gregorič , Martin Rigler , Thomas Müller , Sebastian Düsing , Jorge Saturno, Andreas Nowak, John Backman , Eija Asmi , Krzysztof Ciupek , Douglas Walker , Maria Gini , Konstantinos Eleftheriadis , Stergios Vratolis , Jeffrey Blair , Ivan Iskra , Kyan Shlipak , Weidong Chen , Goufrane Abichou , Yongyong Hu , Jošt V. Lavrič, Johannes Murg , Michael Arndt , Alejandro Keller , Ernest Weingartner & Konstantina Vasilatou (22 Jun 2026): Laboratory-based calibration procedure for filter-based absorption photometers using photothermal interferometry and the extinction-minus-scattering method, Aerosol Science and Technology, DOI: 10.1080/02786826.2026.2688312

To link to this article: https://doi.org/10.1080/02786826.2026.2688312

AEROSOL SCIENCE AND TECHNOLOGY
https://doi.org/10.1080/02786826.2026.2688312

Laboratory-based calibration procedure for filter-based absorption photometers using photothermal interferometry and the extinction-minus-scattering method

Tobias Hammer[a], Luka Drinovec[b,c], Griša Močnik[b,c,d], Asta Gregorič[b,e], Martin Rigler[e], Thomas Müller[f], Sebastian Düsing[f], Jorge Saturno[g], Andreas Nowak[g], John Backman[h], Eija Asmi[h], Krzysztof Ciupek[i], Douglas Walker[i], Maria Gini[j], Konstantinos Eleftheriadis[j], Stergios Vratolis[j], Jeffrey Blair[k], Ivan Iskra[k], Kyan Shlipak[k], Weidong Chen[l], Goufrane Abichou[l], Yongyong Hu[l], Jošt V. Lavrič[m], Johannes Murg[n], Michael Arndt[n], Alejandro Keller[o], Ernest Weingartner[o], and Konstantina Vasilatou[a]

[a]Laboratory of Particles and Aerosols, Federal Institute of Metrology METAS, Bern, Switzerland; [b]Center for Atmospheric Research, University of Nova Gorica, Nova Gorica, Slovenia; [c]Haze Instruments d.o.o, Ljubljana, Slovenia; [d]Department of Environmental Sciences, Jozef Stefan Institute, Ljubljana, Slovenia; [e]Aerosol d.o.o, Ljubljana, Slovenia; [f]Atmospheric Microphysics Department, Leibniz Institute for Tropospheric Research, Leipzig, Germany; [g]Physikalisch-Technische Bundesanstalt, Braunschweig, Germany; [h]Finnish Meteorological Institute, Helsinki, Finland; [i]National Physical Laboratory, Air Quality and Aerosol Metrology Group, Teddington, UK; [j]Environmental Radioactivity & Aerosol Tech. Lab for Atmospheric & Climate Impacts, INRaSTES, National Centre of Scientific Research "Demokritos", Athens, Greece; [k]AethLabs, San Francisco, California, USA; [l]Laboratoire de Physicochimie de l'Atmosphère, Université du Littoral Côte d'Opale, Dunkerque, France; [m]Acoem GmbH, Halle (Saale), Germany; [n]AVL List GmbH, Graz, Austria; [o]University of Applied Sciences Northwestern Switzerland, Windisch, Switzerland

ABSTRACT

We compared aerosol light absorption measurements by a photothermal interferometer (PTI) and by extinction minus scattering (EMS) in a laboratory setting using test aerosols with single scattering albedo (SSA) in the range from about 0.1 to 1. The EMS method reported higher light absorption coefficients, b_{abs}, by 25% up to a factor of 2 compared to PTI, with the deviation increasing when coating fresh soot with secondary organic matter. In a second step, the attenuation measured by numerous filter-based absorption photometers and in-situ-measuring instruments was calibrated against PTI at the wavelengths of 450 and 808 nm to determine reliable calibration factors for each instrument. The attenuation coefficient measured by the filter-based instruments, b_{atn}, was larger by a factor of 4 – 9 than the reference b_{abs} measurements of PTI depending on the instrument model and filter tape. We determined similar multiple-scattering correction factors C for the aethalometer AE33 to those reported by recent studies using PTI as a reference method, but almost two times higher than those reported by older studies referenced to the Multi-Angle Absorption Photometer (MAAP). In-situ-measuring instruments showed a reasonable agreement with PTI despite the low aerosol absorption coefficients which were close to the limit of detection for some of the photoacoustic instruments. In view of the revised Air Quality Directive of the European Union, our study highlights the need for traceable aerosol light absorption measurements to harmonize calibration procedures across Europe.

GRAPHICAL ABSTRACT

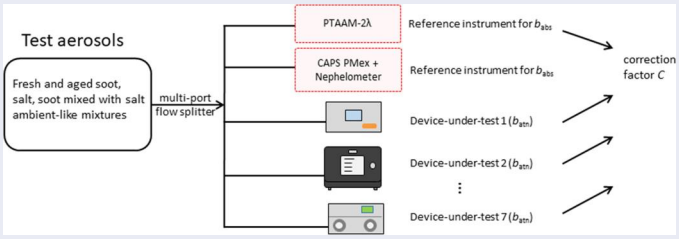

ARTICLE HISTORY

Received 9 March 2026
Accepted 28 May 2026

EDITOR

Hans Moosmüller

CONTACT Konstantina Vasilatou konstantina.vasilatou@metas.ch Laboratory of Particles and Aerosols, Federal Institute of Metrology METAS, Bern, 3003, Switzerland.

Supplemental data for this article can be accessed online at https://doi.org/10.1080/02786826.2026.2688312.

1. Introduction

Black-carbon-containing particles are highly light-absorbing and can thus perturb the Earth's radiative balance either directly (Haywood and Shine 1995) or semi-directly through alteration of atmospheric circulation and cloud cover (Koch and Del Genio 2010). They can also cause adverse health effects due to toxic substances deposited on the BC particle surface (Niranjan and Thakur 2017). As a result, the revised Air Quality Directive of the European Union now mandates the measurement of black carbon mass concentration at selected monitoring stations (European Parliament 2024). Filter-based absorption photometers, already integrated into many atmospheric and air quality networks in Europe and worldwide, provide data relevant to this regulatory requirement. These instruments measure the attenuation of light transmitted through a particle sample collected on a filter. The signal is first converted into the aerosol absorption coefficient (b_{abs}) using a built-in multiple-scattering correction factor, C, which accounts for the optical properties of the filter. An additional correction is often applied that accounts for systematic artifacts arising from increasing filter loading (i.e., progressive filter darkening) causing a decrease in sensitivity of the measurement. In a second step, the equivalent black carbon (eBC) mass concentration is derived using a built-in mass absorption cross-section (MAC). Both C and MAC are treated as constants by the instrument, but in practice they depend on both time- and site-specific aerosol properties, such as mixing state and particle size (Renzi et al. 2025).

In particular, C accounts for the enhanced light attenuation and extended optical path length caused by multiple scattering within the filter matrix. This correction is primarily dependent on the physical and optical properties of the filter material used in a given filter-based photometer. In the absence of an independent calibration method, efforts for harmonization relied on intercomparison studies, where the multi-scattering correction factor was derived from the systematic bias remaining when the loading correction was efficiently applied. This was the case in earlier studies targeting to resolve the issue for the AE31 aethalometer, with a C factor of 3.5 (Backman et al. 2017; Müller and Fiebig 2018) and the AE33 aethalometer with a harmonization factor of 1.75 (Savadkoohi et al. 2024). Although current instruments apply a constant, wavelength-independent C value, recent studies indicate that C may vary as a function of aerosol single scattering albedo (SSA) (Yus-Díez et al. 2021), particle size distribution (Moteki et al. 2010; Nakayama et al. 2010; Renzi et al. 2025), and mixing state (Müller et al. 2011). These dependencies arise from the aerosol optical properties and their interactions with the fibrous structure of the filter substrate. Smaller particles (approx.$<$150 nm) differ from larger ones by their ability to penetrate deeper into the filter matrix, increasing the effective optical path length and enhancing multiple scattering, which leads to higher C values. Cross-sensitivity to scattering, which is more pronounced at shorter wavelengths, further affects the attenuation coefficient measured by filter-based photometers, as extensively discussed by Yus-Diez (2021, 2025).

Unlike C, which primarily depends on the interaction between deposited particles and the filter matrix, the mass absorption cross-section (MAC) introduces a fundamentally different source of uncertainty in eBC determination. MAC links measured absorption to equivalent black carbon mass and reflects variability in the aerosol composition, driven by atmospheric aging, coating thickness, and lensing effects (Yuan et al. 2021; Zhao et al. 2021).

Although C and MAC are conceptually distinct, their combined variability strongly influences the accuracy of eBC mass measurements. For smaller particles, C tends to increase, leading to higher measured attenuation, whereas MAC generally decreases with particle size (Mehri et al 2025). These opposing trends partially offset each other, resulting in a lower overall variability in the reported eBC mass concentration compared to the variability of each parameter individually. In contrast, coated particles introduce a different effect: both C and MAC increase—C due to enhanced multiple scattering within the filter and MAC due to absorption enhancement from the lensing effect. This simultaneous increase amplifies the bias and can lead to significant overestimation of eBC concentrations. Therefore, accurate eBC mass determination requires calibration of both parameters C and MAC—rather than adjusting only one. Filter-based absorption photometers need to be calibrated against reference methods with well-known measurement uncertainties using test aerosols of different mixing states that cover the whole single scattering albedo (SSA) range.

In situ methods for measuring light absorption, such as photoacoustic/photothermal spectrometry and extinction-minus-scattering (EMS), have often been used in the past as reference methods for characterizing filter-based photometers (Petzold et al. 2013; Kalbermatter et al. 2022). Photoacoustic spectrometers (PAS) (Tomoki Nakayama et al. 2015) and photothermal interferometers

(PTI) (Sedlacek 2006; Drinovec et al. 2022) measure b_{abs} directly by illuminating particles with a powerful modulated or pulsed pump light source (Sharma et al. 2013). The light absorbed by the aerosol is converted to heat, causing a modulated increase in local temperature and changes in air density. PAS and PTI detect the generated acoustic waves and the change in the refractive index of the air, respectively (see (Nakayama et al. 2015; Drinovec et al. 2022) and references therein). PTI measurements are not sensitive to the sample properties (Drinovec et al. 2022), while PAS measurements are affected by the particle size distribution (Cremer et al. 2017).

EMS relies on separate measurements of the aerosol extinction and scattering coefficients that can either be performed by the same instrument (e.g. a cavity-attenuated phase-shift single-scattering albedo monitor, CAPS PMssa, Droplet Measurement Technologies DMT, USA) or a combination of an extinctiometer (e.g. a CAPS extinction instrument, CAPS PMex, DMT, USA) and a nephelometer (Onasch et al. 2015); the absorption coefficient is then calculated as the difference between these two parameters. Since EMS is an indirect method for determining the aerosol light absorption coefficient, care must be taken when measuring high-SSA aerosols. Although the scattering and extinction coefficients can be measured with high accuracy (i.e., with uncertainties on the order of 1–10%), the corresponding uncertainties in EMS-derived absorption may range from about 10 % to larger than 100 % at high SSA values (Singh et al. 2014; Foster et al. 2019; Modini et al. 2021). It must be pointed out that the nephelometer response is a function of the refractive index of the particles (Massoli et al. 2009) and the truncation correction of the instrument (i.e., accounting for the near-forward and near-backward scattered light that remains undetectable by the instrument) depends on the aerosol sample properties, such as the size distribution. Detailed information on the factors affecting the performance of nephelometers and EMS can be found in Modini et al. (2021).

A significant advantage of *in situ* methods is that they can be calibrated with reference gases at short wavelengths (i.e., near-ultraviolet and lower-visible range), where species such as NO_2 or ozone have well- characterized absorption cross sections (Arnott et al. 2010; Nakayama et al. 2015; Davies et al. 2018). At longer (infrared) wavelengths, calibration can be performed using light-absorbing particles such as soot (Tomoki Nakayama et al. 2015), Aquadag (Foster et al. 2019), nigrosin (Bluvshtein et al. 2017; Foster et al. 2019), light-absorbing polystyrene spheres (Lack et al. 2006) or ambient oxygen (Corbin et al. 2025).

Although *in situ* absorption instruments are available, the filter-based Multi-Angle Absorption Photometer (MAAP, Fisher Scientific) remains widely used as a pseudo-reference instrument, e.g., within the Aerosol, Clouds and Trace Gases Research Infrastructure in Europe (ACTRIS). The MAAP has been shown to report absorption coefficients of up to 50% higher than PTI (PTAAM-2λ, Haze Instruments, Slovenia). (Kalbermatter et al. 2022; Yus-Díez et al. 2025) and up to 30% higher than EMS (Modini et al. 2021). As a result, multiple scattering correction factors C for the AE33 Aethalometer determined based on the MAAP are significantly smaller than those determined based on the PTI method (Yus-Díez et al. 2025).

Despite the lack of standardized methods for calibrating filter-based absorption photometers, several comparisons with in-situ reference methods using fresh and aged soot particles have been reported in past studies (see, for instance, (Kalbermatter et al. 2022) and references therein). Fresh soot particles are typically generated by a combustion generator (see (Ess and Vasilatou 2019; Ess et al. 2021) and references therein), and can be further coated with primary organic matter (Salo et al. 2024). Aged particles can be generated by coating soot with secondary organic (Ess et al. 2021; Kalbermatter et al. 2022; Leni et al. 2022) or inorganic matter (Salo et al. 2024). The filter-based photometer calibration factors depend on particle size, coating thickness and the wavelength of the light source (Drinovec et al. 2022; Kalbermatter et al. 2022).

The goal of this work was three-fold:

i. to compare the EMS and PTI reference methods for aerosol light absorption and determine experimentally-derived measurement uncertainties for EMS at high SSA,
ii. to extend the laboratory-based calibration method reported by Kalbermatter et al. (2022) based on fresh and aged soot particles to well-defined PM_1 ambient-like aerosols and mixtures of salt and soot in order to determine reliable multiple scattering calibration factors C for filter-based photometers, and
iii. to assess the applicability of the MAAP, custom-made PAS and commercial PAX (Photoacoustic extinctiometer) instruments as secondary standards for aerosol light absorption.

To this end, different commercially available high-end and mid-cost filter-based absorption photometers and *in situ* measuring monitors were calibrated against the EMS and PTI methods and reliable

calibration factors with respect to light absorption were obtained in the SSA range from about 0.1 to 1.

2. Methods

2.1. Aerosol generation

A schematic illustration of the experimental setups is shown in Figures 1 and 2. Fresh (uncoated) soot was generated with a miniCAST 5201 Type BC (Jing Ltd., Switzerland) combustion generator (Ess and Vasilatou 2019; Ess et al. 2021). The soot particles were first diluted with particle-free air by a factor of 10:1 using an eDiluter (Dekati, Finland) and then coated with secondary organic matter (SOM) from the ozonolysis of α-pinene vapors using the organic coating unit (OCU, University of Applied Sciences North-Western Switzerland, Switzerland) (Keller et al. 2022). For the experiments with uncoated soot, the OCU was bypassed. The aerosols were further diluted using a rotational disk diluter (MD19, Matter Engineering AG, Switzerland), and additional filtered air was added using a mass flow controller (MFC) to increase the aerosol flowrate. The aerosols were delivered to the measuring instruments through a custom-made 12-port flow splitter. Since the sampling flowrates of the different instruments ranged from 0.15 L min^{-1} to 10 L min^{-1}, isokinetic sampling ports were designed to ensure representative sampling even for micrometre-sized particles (see experiments with ambient-like aerosols described below). Differences in diffusion losses were compensated for by adjusting the length of the connecting tubes to the sampling flow of the instruments. Limitations related to the flowrate and aerosol concentration required the separation of the measuring instruments (reference instruments and devices under test, DUT) into three groups. Inorganic salt (i.e., ammonium sulfate) aerosols were generated with an ATM 220 nebulizer (Topas GmbH, Germany) and dried with a Nafion dryer (model MD-700-12S-1, PERMA PURE, UK). For generating size distributions with GMD_{mob} larger than 100 nm, the salt aerosols were passed through an agglomeration tube (i.e., a simple metallic tube). The salt aerosols were diluted and delivered directly to the measuring instruments (see Table S1 in the online supplementary information [SI]). Alternatively, 150 nm salt particles were mixed with soot particles (GMD_{mob} of 75 nm) to produce mixtures of salt and soot particles (path b of Figure 1). The generated mixtures had a relative humidity (RH) of 6 – 8% (same as the other aerosols produced in this study), and the ratio of internally to externally mixed particles was about 1:1.

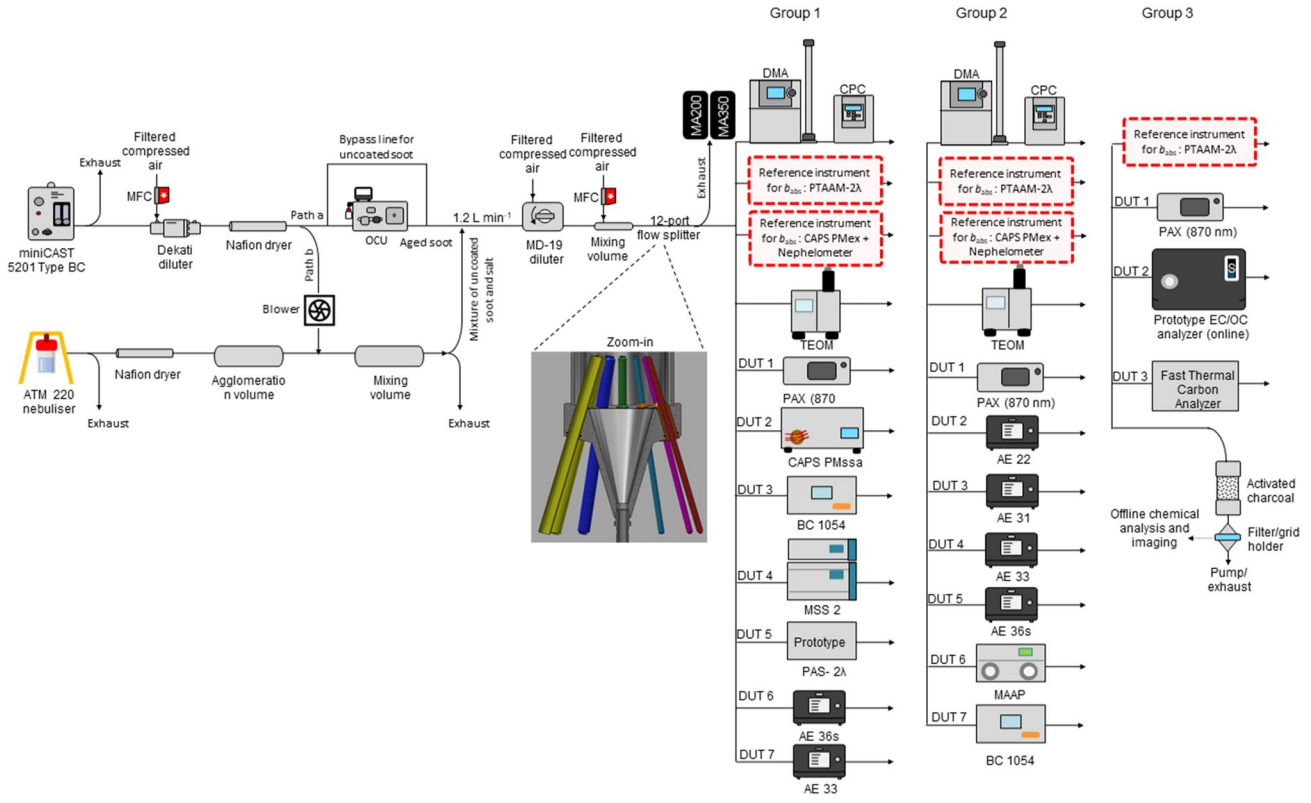

Figure 1. Schematic illustration of the experimental setup for the generation of fresh and aged soot (path a), ammonium sulfate and mixtures thereof (path b). The measuring instruments were split into 3 groups due to limitations in the generation of aerosol flows at the required particle number concentrations. The results of the Fast Thermal Carbon Analyer known as the FATCAT and the prototype EC/OC analyzer will be reported in a separate publication.

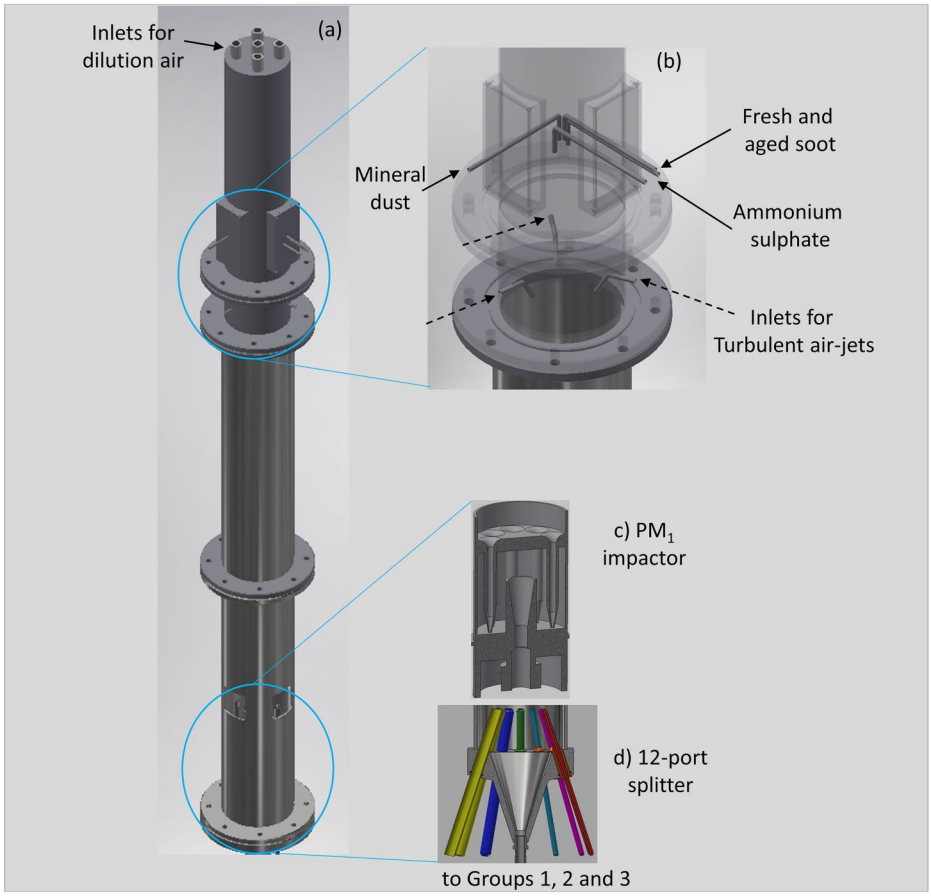

Figure 2. Schematic representation of the experimental setup for the generation of ambient-like aerosols with the facility known as PALMA (Horender et al. 2021). Panel (a) depicts a vertical aerosol hologenizer with inlets for dilution air at the top. Panel (b) provides a close-up, showing inlets for turbulent air-jets, fresh soot, aged soot, mineral dust and ammonium sulfate. Panel (c) features a PM_1 impactor. Panel (d) illustrates a custom-made 12-port flow splitter.

Table 1. Summary of the test aerosols generated in this study.

Aerosol series nr.	Aerosol composition (GMD_{mob})		
A1	Fresh soot – size 1 (75 nm)	Soot with thin SOA coating (92 nm)	Soot with thick SOA coating (117 nm – 121 nm)
A2	Fresh soot – size 2 (108 nm)	Soot with thin SOA coating (136 nm – 138 nm)	Soot with thick SOA coating (152 nm – 165 nm)
A3	Soot internally and externally mixed with ammonium sulfate (90 nm)		
A4	Ammonium sulfate (four particle sizes, 84 nm – 147 nm)		
A5	PM_1 ambient-like aerosol (i.e., fresh and aged soot, ammonium sulfate and fine mineral dust, 147 nm)		

Ambient-like aerosols, i.e., homogeneous mixtures of fresh and aged soot, ammonium sulfate and mineral dust particles were generated with the setup known as PALMA as described in (Horender et al. 2021; Stefan Horender et al. 2021). Briefly, fresh soot particles were generated with a miniCAST 6204 burner (Jing Ltd., Switzerland). Part of the combustion aerosol (soot) was aged with SOM from the ozonolysis of α-pinene using an oxidation flow reactor known as the Micro Smog Chamber ((Keller and Burtscher 2012; Ess et al. 2021), see also (Keller et al. 2022) for an automated version of the Micro Smog Chamber). Salt particles were generated by nebulizing an aqueous solution of ammonium sulfate with a TSI 3076 atomizer (TSI Inc., USA). Mineral dust particles (ISO 12103–1 A2 fine test dust, Powder Technology Inc., USA) were generated with a rotating-brush generator (RBG 1000, Palas, Germany). The typical geometric mean diameters of these aerosols were 90 nm, 110 nm, 70 nm and 150–200 nm, respectively. The aerosols were injected into a 3-m-long vertical tube (homogenizer) through separate inlets and mixed by three turbulent air-jets as shown in Figures 2a and b. The aerosols (RH <10%) were sampled by the measuring instruments through a PM_1 impactor (Digitel, Switzerland) and the custom-made 12-port flow splitter (Figure 2c) and the measurement instruments as described above.

The test aerosols generated in this study are listed in Table 1. Their physical properties were investigated

with an array of methods as described in Section 2.3 and are listed in SI Table S1.

2.2. Instruments measuring light absorption

All three groups of aerosol-measuring instruments (Figure 1) included the latest version of the dual-wavelength Photothermal Aerosol Absorption Monitor (PTAAM-2λ, Haze Instruments d.o.o., Slovenia), a PTI instrument operating at wavelengths $\lambda = 450$ nm and $\lambda = 808$ nm (Yus-Díez et al. 2025), as reference instrument for light absorption. The instrument was calibrated with NO_2 and nigrosin particles as described in Drinovec et al. (2022). The second reference setup for aerosol light absorption based on the EMS method consisted of 3 different CAPS $PM_{ex,}$ monitors (DMT, USA) and a polar integrating nephelometer Aurora 4000 (ACOEM, France). Two of the CAPS $PM_{ex,}$ monitors operated at $\lambda = 630$ nm and the other at $\lambda = 450$ nm, while the nephelometer featured wavelengths $\lambda = 450$ nm, $\lambda = 525$ nm and $\lambda = 630$ nm.

The calibration of EMS systems requires calibration of two instruments. In a first step, the nephelometer Aurora 4000 (ACOEM, France) was calibrated with a gas of known scattering cross section, and in a second cross-calibration, the extinction cell was cross-calibrated against the nephelometer using non-absorbing light scattering aerosols. An absolute calibration of the extinction cell for the used CAPS PMex monitors is generally not possible because the effective path length in the multiple reflection cavity with a sheath air layer protecting the mirrors is not precisely known. Instrumental uncertainties, which depend on the properties of the gases and aerosol, require correction of the data for calibration and must also be taken into account for different aerosol types in the application.

Nephelometers are usually calibrated with CO_2 as the light scattering cross section for wavelengths between 450 nm and 700 nm is well known (Anderson et al. 1996). Furthermore, the instrument intensity transfer function for Aurora nephelometers is given in Müller et al. (2011) allowing calculation of the truncation error for gases or aerosols of known phase functions.

Since CAPS PMex cannot be calibrated directly using a known quantity of certified gases or aerosols, cross-calibration is performed. In practice, this means that the effective path length factor is determined so that the light scattering coefficients measured by nephelometer and the extinction coefficients measured by CAPS PMex for non-absorbing aerosols, in this case ammonium sulfate, match. To keep truncation artifacts low, small particles with a high scattering Ångström exponent (SAE) of about 3 were generated with an atomizer and dried. The truncation correction for this cross-calibration can be corrected using a parametrisation according to Müller, Laborde, et al. (2011).

When using the method to derive the absorbing aerosol, two key aspects of EMS techniques must be taken into account. At low concentrations, the difference between extinction and scattering is small, and absorption becomes uncertain due to instrument noise. Furthermore, at high single scattering albedos (e.g. >0.6), the difference is small, and uncertainties in the truncation correction lead to uncertainty in the absorption coefficient. The uncertainty of EMS methods and their application limits are discussed in detail in Romshoo et al. (2025, to be submitted).

The DUT comprised different commercially available high-end and mid-cost filter-based photometers, such as the Aethalometer (models AE22, AE31, AE33, AE36s, Aerosol Magee Scientific, Slovenia), the microAethalometer (models MA200 and MA350, AethLabs, USA), the BC 1054 multi-wavelength black carbon analyzer (Met One, USA), and the multi-angle absorption photometer (MAAP 5012, Thermo Scientific, USA), and *in situ* measuring monitors, such as the photoacoustic extinctiometer (PAX-870-T, DMT, USA), the micro soot sensor (MSS2, AVL, Austria) and a prototype photoacoustic sensor PAS-2λ measuring at 450 nm and 880 nm (Université du Littoral Côte d'Opale, France). All instruments were either serviced and tested by the manufacturer or on-site following the calibration procedures documented in the respective manuals. The flow rates of the DUT have a significant impact on the measured absorption and were therefore regularly checked using a bubble flow meter known as the Gilibrator 2 (Lauper Instruments AG, Switzerland) that has an accuracy of ±3%. Table S2 provides an overview of the instruments used in this study along with their main technical characteristics.

2.3. Aerosol characterization

Aerosol mobility size distributions were measured using a scanning mobility particle sizer, SMPS (Electrostatic Classifier Series 3080 with ^{85}Kr radioactive source, a DMA column 3082 and a CPC 3752, TSI Inc., USA) as shown in Figure 3. Geometric mean mobility diameter (GMD_{mob}), volume mean equivalent diameter (D_v) and total particle number concentration were determined from the particle size

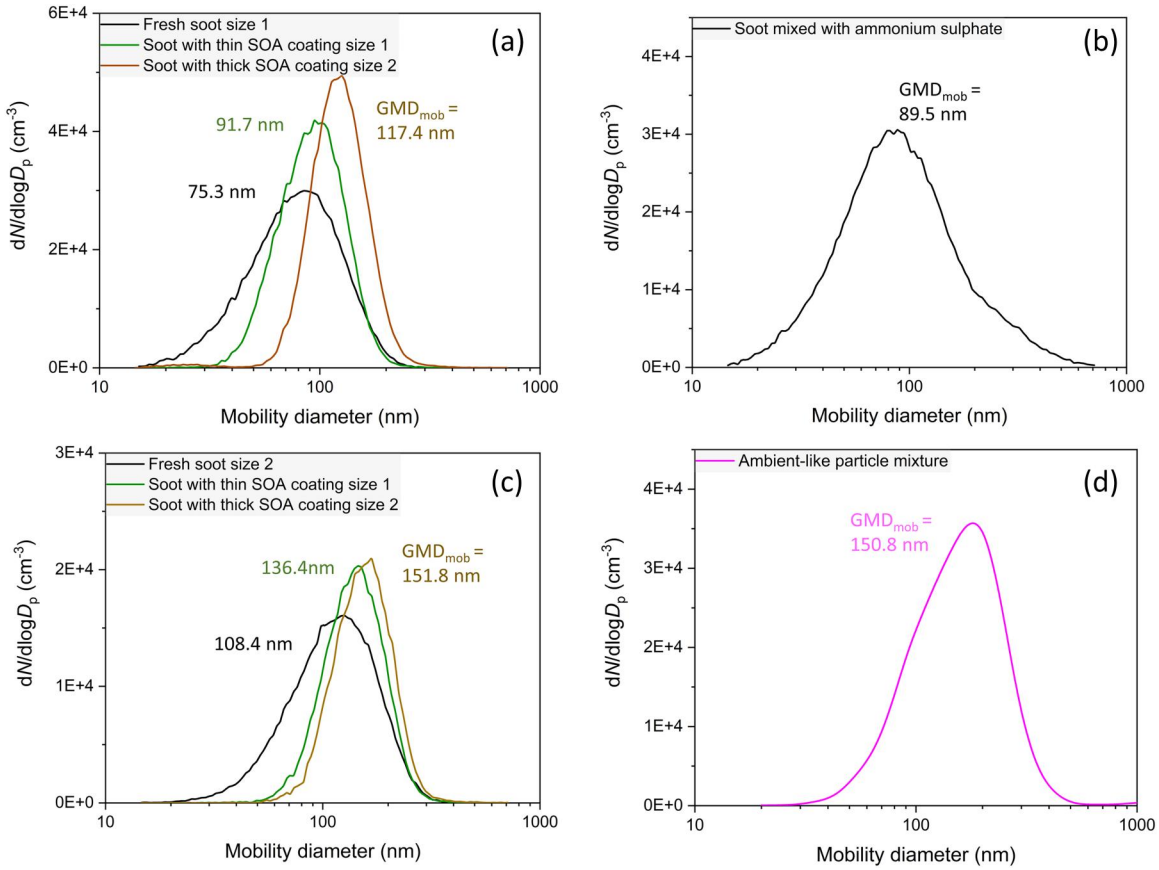

Figure 3. Number-based mobility size distributions of the test aerosols for Group 1.

distribution using the software provided by the manufacturer (Aerosol Instrument Manager, v 9.0.0.0, TSI Incorporated, USA).

The ratio of the total number concentrations between the different operation points was used for scaling the b_{abs} values reported by the BC-measuring instruments to correct for inter-day drifts and day-to-day variability. Moreover, a tapered-element oscillating microbalance (TEOM 1405, Thermo Fisher Scientific Inc., USA) was used to measure total aerosol mass concentrations. The TEOM was operated at a flow of 2.7 L min^{-1} and the temperature was reduced to 30 °C to avoid loss of volatile SOM from the soot surface.

Thermal–optical analysis was performed with a Lab OC–EC aerosol analyzer (Sunset Laboratory Inc., USA). Aerosols were sampled on two superimposed filters for each measurement point (Group 3 in Figure 1). For the coated samples, the aerosol was passed through an activated-charcoal denuder first. The filters (47 mm QR-100 quartz-fiber filters, Advantec, Japan, prebaked at 500◦C for 2 h) were placed in a metallic filter holder (Merck Millipore, Germany). The Lab OC–EC aerosol analyzer separated carbonaceous material into EC and OC (elemental and organic carbon, respectively) based on the EUSAAR2 protocol (Cavalli et al. 2010). The latter was slightly modified by extending the last temperature step to ensure that the evolution of carbon is complete (Ess and Vasilatou 2019). OC and EC masses were determined from the upper filter, and OC masses were later corrected by subtracting the mass of OC from the lower filter, corresponding to the mass of the absorbed gas phase. In addition, the total carbon content in aerosols (TC) and its subgroups (EC and OC) was measured using FATCAT (Keller et al. 2023) and a prototype EC/OC analyzer by Sunset Lab. The results obtained with these devices will be presented in detail in a separate publication.

The main properties of the generated aerosols are summarized in Table S1. The AAE was determined from the PTAAM-2λ measurements at the two available wavelengths of 450 nm and 808 nm. The SSA was determined in two ways:

1. at 450, 630 and 870 nm based on the EMS and PAX measurements
2. at 450 nm and 808 nm by combining the b_{scat} values from the nephelometer and the b_{abs} values measured with PTAAM-2λ.

To obtain the SSA value at 808 nm, the b_{scat} value from the nephelometer at 635 nm was converted to 808 nm using the scattering Ångström exponent (SAE) calculated based on the measurements at 450 nm and 635 nm.

In the case of soot and salt mixtures, the particles were collected on copper-coated TEM grids (Agar Scientific, UK) using a mini particle sampler (MPS, Ecomesure, France). Transmission electron microscopy (TEM) images were recorded with a Spirit TEM instrument (Tecnai, FEI Company, USA) with a measurement voltage of 80 kV.

TEM was used to investigate the morphology of the soot (GMD_{mob}=75 nm) and ammonium sulfate (GMD_{mob}=150 nm) aerosol mixtures (see Table 1). The size distribution of the aerosol mixture had a GMD_{mob} of about 90 nm. The TEM images reveal that the particles were both internally and externally mixed (Figure 4). Based on about 200 particles, we estimated the ratio of internally to externally mixed particles to be roughly about 1:1. Most ammonium sulfate particles appeared as cubic-shaped crystals; however, a few spherical ammonium sulfate particles were also observed (Figure 4c), which likely correspond to encapsulated soot. The morphology of the internally mixed particles reproduced well that of ambient soot and salt mixtures sampled at different locations in China (Wang et al. 2017).

3. Results

3.1. Comparison of the reference methods

The two reference methods, EMS (CAPS PMex and nephelometer) and PTI (PTAAM-2λ), were compared using the test aerosols listed in SI Table S1a. In Figure 5a, the absorption coefficient reported by the EMS method is plotted against the measurement of the PTAAM-2λ at 450 nm. The measurements were performed with the test aerosols A1-A3 and A5 listed in Table 1. The SSA values of the different aerosols are shown as data labels. In the visible/near UV region of the spectrum, the two reference methods in most cases did not agree within the stated

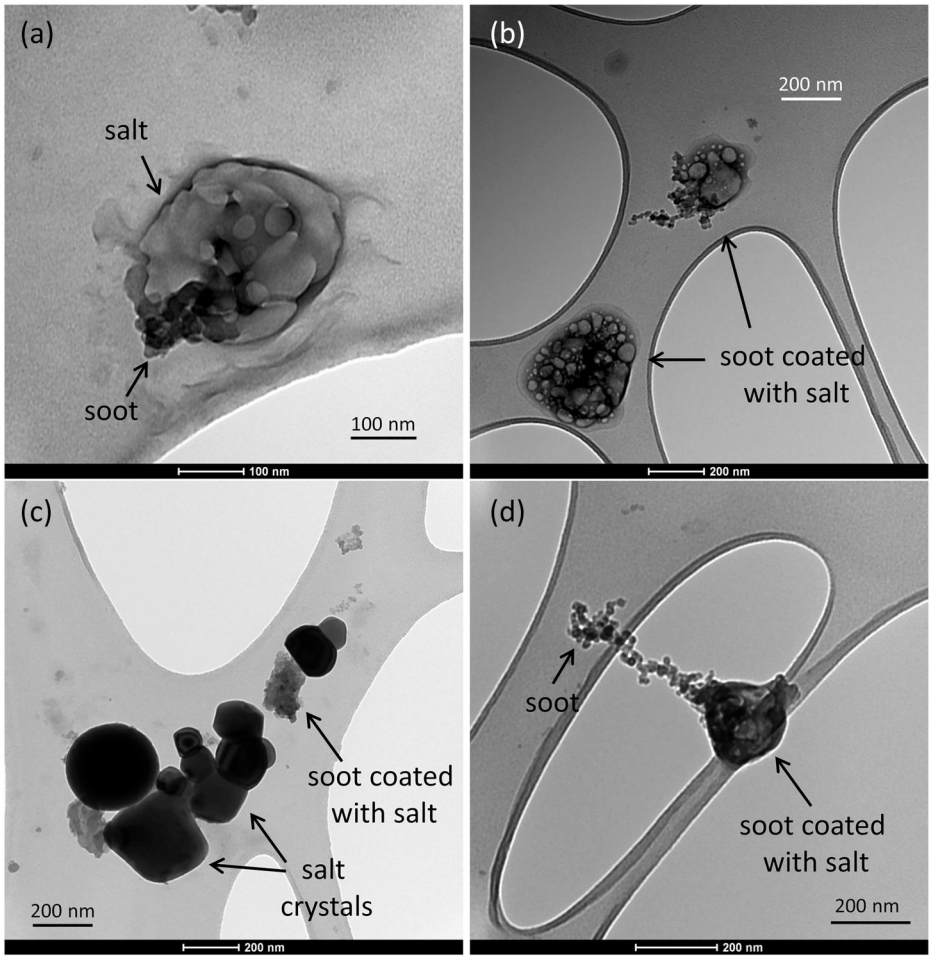

Figure 4. TEM images of soot and ammonium sulfate mixtures: (a) and (b) soot internally mixed with ammonium sulfate and (c) and (d) soot externally mixed with ammonium sulfate particles.

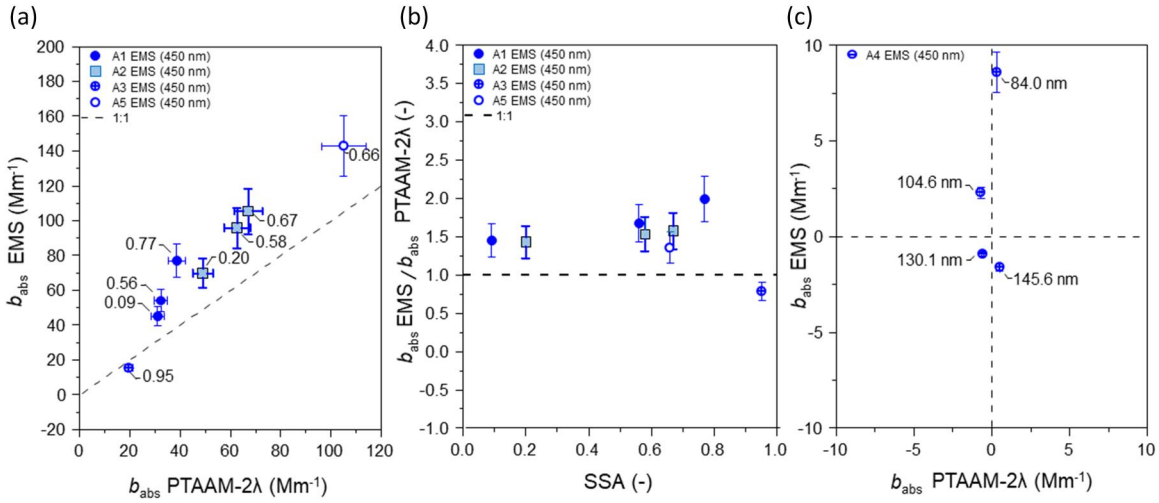

Figure 5. (a) Comparison of the absorption coefficient b_{abs} reported by the EMS method (450 nm) and the PTAAM-2λ (450 nm) for aerosols A1, A2, A3 and A5 (Table 1). Data labels indicate SSA. (b) Ratio of the absorption coefficients b_{abs} reported by the EMS method (450 nm) and the PTAAM-2λ (450 nm) in the visible wavelength range for aerosols A1, A2, A3 and A5 as a function of the aerosol SSA. c) Comparison of the absorption coefficient b_{abs} reported by the EMS method (450 nm) and the PTAAM-2λ (450 nm) for purely scattering aerosol A4 (ammonium sulfate particles, SSA = 1). Data labels indicate GMD_{mob}. The dashed lines in panels (a) and (b) represent the 1:1 instrument response to guide the eye. The dashed line in panel (c) represents a b_{abs} value of zero expected for a purely scattering aerosol. In all panels, the error bars designate expanded measurement uncertainties ($k = 2$).

uncertainties (see SI Table S3), with the magnitude of the deviation depending partly on the aerosol SSA. Previous experiments carried out at the Leibniz Institute for Tropospheric Research (TROPOS) had revealed a better agreement between the two methods (typically within 10% for SSA up to about 0.5, see Deliverable 3 of the StanBC project available at: https://stanbc.com/documents-and-publications). EMS has a complex and sensitive set up. The larger deviations between EMS and PTI observed in our study might be due to the fact that EMS was run by a different operator in a different laboratory.

To investigate the dependence of the EMS measurements on the SSA, the data are plotted in Figure 5b as the ratio of the b_{abs} reported by EMS to b_{abs} of the PTAAM-2λ. For both aerosols A1 and A2, where fresh soot was progressively coated with SOM, the deviation in b_{abs} measured by EMS increased with increasing SSA from ~50% at an SSA ≈ 0.09 up to ~100% at an SSA ≈ 0.77, with EMS overestimating b_{abs} relative to PTAAM-2λ. However, at an SSA ≈ 0.95, the measurement of test aerosol 3 (soot mixed with ammonium sulfate) yielded b_{abs} values from EMS lower than those reported by PTAAM-2λ.

The response of the two reference methods to purely scattering aerosols (A4, ammonium sulfate) is shown in Figure 5c. Here, b_{abs} reported by the EMS (450 nm) has not been converted to 808 nm as the AAE for a highly scattering aerosol such as ammonium sulfate is not well defined. Ammonium sulfate particles do not absorb light and the absorption coefficient should be zero. Indeed, the PTAAM-2λ measured values close to zero at both wavelengths, while EMS measured positive b_{abs} values for the smallest particle sizes (GMD_{mob}≈84 and 104.6 nm, see data labels) in the visible/near UV region. The data presented in all panels of Figure 5 are summarized in SI Table S4.

The uncertainty budget of each method for a given wavelength is given in SI Table S3. The measurement accuracy of the EMS method depends on the quality of extinction and scattering measurements:

a. Scattering is affected by the truncation error. The truncation correction is only optimized for certain types (e.g., size) of particles, and the error increases with increasing aerosol SSA;
b. The extinction measurements may be affected by contamination of the CAPS PMex optical windows resulting from pressure changes during the experiment. In this case, the CAPS PMex should be recalibrated. Depending on the calibration and truncation errors, the combined error in the measurement of b_{abs} at high SSA can be positive or negative. In our study, no contamination of the PMex windows was observed.

To summarize, in the visible/near UV region the EMS method reported higher absorption coefficients than the PTAAM-2λ by up to a factor of 2, with the measurement deviation increasing with increasing SSA when coating fresh soot with SOA. This is in line

with past studies (Foster et al. 2019; Modini et al. 2021). According to Modini et al. (2021): "Care must be taken with EMS measurements due to the occurrence of large subtractive error amplification, especially for the predominantly scattering aerosols that are typically found in the ambient atmosphere. Practically, this means that although the CAPS PMssa can measure scattering and extinction coefficients with high accuracy (errors on the order of 1–10%), the corresponding errors in EMS-derived absorption range from 10% to greater than 100%". Foster et al. report that the % error in absorption reported by the EMS method (CAPS PMssa) should approach 5% as SSA approaches zero, but the error reaches infinity as the SSA approaches 1.

The measurements in the red region of the visible spectrum are presented in Figure S1 (red data sets). At this wavelength (630 nm), the EMS method did not exhibit the expected behavior, i.e., error increasing with increasing SSA. Instead, the agreement with the PTAAM-2λ was satisfactory at SSA $\leq$0.59, but EMS reported negative values for all test aerosols with higher SSA (soot mixed with ammonium sulfate particles and pure ammonium sulfate). As we do not have a clear explanation for this behavior and cannot rule out the possibility of a technical issue, we chose to present the measurements in the SI.

3.2. Calibration of aerosol light absorption against the PTAAM-2λ

This study focuses on the calibration of filter-based absorption photometers designed for atmospheric research and air quality monitoring rather than engine emission control. Since ambient aerosols exhibit SSA values larger than 0.6 even in polluted urban centers (Devi and Satheesh 2022; Ganguly et al. 2006), we will use hereafter the PTAAM-2λ as reference instrument while acknowledging at the same time the potential of the EMS method to serve as reference at SSA values below ~0.6.

The ratio of the attenuation coefficient, b_{atn}, measured by the filter-based absorption photometers to the reference b_{abs} measurements by the PTAAM-2λ is plotted as a function of the aerosol SSA in Figure 6. All b_{atn} values have been converted to a wavelength of 450 nm (panels a and b) and 808 nm (panels c and d) using the absorption Ångström exponents (AAE) determined from the fit over the two b_{abs} values from the PTAAM-2λ (see SI Table S1). A comparison with the AAE values obtained from similar wavelength pairs of the filter-based instruments is shown in Table S5. The b_{atn} have also been corrected with respect to particle number concentration, which was slightly different between different runs. Note that some of the measurements were repeated twice for instrument Groups 1 and 2 as explained in Section 2.1, and the SSA of the test aerosols was similar but not necessarily identical between the two runs. The statistical measurement uncertainties of the devices-under-test were $\leq$4% (standard deviation for a coverage factor $k=2$) while the combined measurement uncertainties of the PTAAM-2λ were 8.4% to 12.4% ($k=2$) as summarized in SI Table S3 and in Yus-Díez et al. (2025). The expanded uncertainty of the calibration factor $b_{abs,\,DUT}/b_{abs,\,PTAAM}$ lies typically below 15% ($k=2$; 95% confidence interval) as will be explained in more detail at the end of Section 3. The uncertainties have not been plotted to improve the legibility of the graphs.

Figure 6 shows that the b_{atn} coefficients of the filter-based instruments were consistently larger than the b_{abs} measured by the PTAAM-2λ by a factor of ~4–9, which corresponds to the calibration multiple-scattering parameter C. The magnitude of C depended significantly on the instrument type/filter tape, as already highlighted by past studies (see, for instance, (Müller et al. 2011; Yus-Díez et al. 2021, 2025) and references therein), but did not seem to strongly depend on the composition of the test aerosol and therefore the aerosol SSA. For both test aerosols A1 and A2, a small increase in the C value is observed after the first coating step with SOM. This might be due to the collapse of the soot core (Keller et al. 2022; Leni et al. 2022), though other factors such as the additional scattering by the coating material (cross-sensitivity to scattering) and multiple scattering in the filter could also play a role.

The tape material of the filter-based absorption photometers used in this study along with the filter tape-specific C values defined by the manufacturers are listed in Table 2. Hereafter, we will denote the filter tape-specific C values defined in the instrument manuals as C_m to distinguish them from the C values (calibration parameters) obtained in this study. The AE33 and AE36/AE36s aethalometers were equipped with M8060 glass fiber filter tapes (C_m=1.39), while the AE22 and AE31 units with Pallflex Q250F quartz filter tapes (C_m=2.14). MA200 and MA350 were equipped with PTFE filters (C_m=1.3) and BC-1054 with proprietary reinforced glass fiber filters (C_m=2.61). The measured C values of all DUT lay

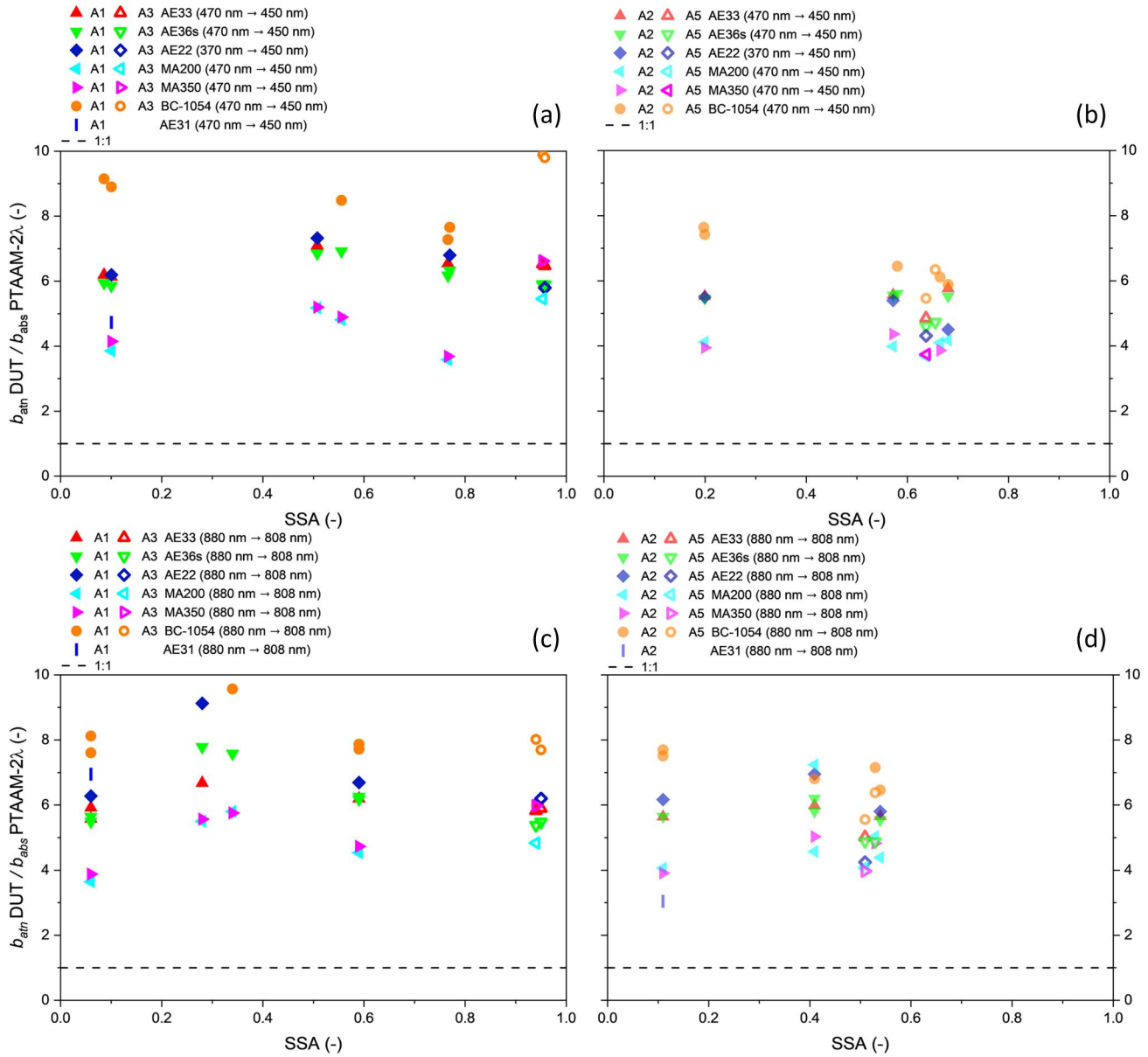

Figure 6. Ratio of the attenuation coefficients b_{atn} reported by the filter-based absorption photometers to the reference b_{abs} values reported by the PTAAM-2λ as a function of SSA determined using the b_{abs} from PTAAM-2λ and the b_{scat} from the nephelometer. Measurements at 450 nm were performed with (a) A1 and A3, and (b) A2 and A5 test aerosols (see Table 1). Likewise, measurements at 808 nm were carried out with (c) A1 and A3, and (d) A2 and A5 test aerosols. For (a) and (b), all b_{atn} values have been converted to a wavelength of 450 nm using the absorption Ångström exponents determined from the fit over the two b_{abs} values from the PTAAM-2λ, whereas for (c) and (d) all b_{atn} values have been converted to a wavelength of 808 nm using the absorption Ångström exponents determined from the fit over the two b_{abs} values from the PTAAM-2λ (Supplemental Table S1). The original measurement wavelengths of the DUTs are indicated in the legend. The dashed horizontal line represents the 1:1 instrument response to guide the eye.

typically in the range 3.7 to 9.9 and 3.0 to 9.6 at 450 nm and 808 nm respectively.

Variability in the C factor (Table 2, Figure 6) was primarily associated with the filter material used in DUT, but also depended on particle size and coating. The highest C values were observed in experiments with bare and coated soot, as well as mixtures of soot with ammonium sulfate (A1–A3). In contrast, ambient-like aerosol produced lower C values (A5), ranging from 3.74 to 5.90 at 470 nm and from 3.96 to 5.96 at 880 nm.

For the experiments with the aerosols A1–A3, the highest C value was obtained for the BC-1054 instrument, averaging 7.83 ± 1.28 at 470 nm and 7.76 ± 0.86 at 880 nm. C values for the AE33 and AE36s instruments (which share the same optical configuration and filter)

Table 2. Overview of the multiple-scattering correction factors *C* obtained in this study for the 450 nm and 808 nm wavelengths of the PTAAM-2λ and the corresponding manufacturer-defined values C_m.

		Groups 1 & 2 (average *C* values[a])						
		C (370 nm, 470 nm → 450 nm)						
		AE33 (470 nm)	AE36s (470 nm)	AE22 (370 nm)	MA200 (470 nm)	MA350 (470 nm)	BC-1054 (470 nm)	AE31[b] (470 nm)
A1	Fresh soot – size 1	6.16	5.91	6.19	3.85	4.14	9.03	4.73
	Soot with thin SOA coating	7.09	6.89	7.32	5.00	5.05	8.49	
	Soot with thick SOA coating	6.55	6.25	6.80	3.58	3.69	7.47	
A3	Soot mixed with ammonium sulfate	6.50	5.90	5.80	5.46	6.62	9.85	
A2	Fresh soot – size 2	5.52	5.45	5.49	4.11	3.93	7.52	
	Soot with thin SOA coating	5.55	5.57	5.38	5.15	4.35	6.44	
	Soot with thick SOA coating	5.75	5.51	4.49	4.13	3.85	5.99	
A5	PM_1 ambient-like aerosol	4.84	4.66	4.30	3.69	3.74	5.90	
		C (880 nm → 808 nm)						
		AE33 (880 nm)	*AE36s (880 nm)*	*AE22 (880 nm)*	*MA200 (880 nm)*	*MA350 (880 nm)*	*BC-1054 (880 nm)*	*AE31 [b] (880 nm)*
A1	Fresh soot – size 1	5.75	5.57	6.28	3.64	3.88	7.87	6.95
	Soot with thin SOA coating	6.68	7.69	9.13	5.65	5.67	9.57	
	Soot with thick SOA coating	6.20	6.22	6.69	4.54	4.73	7.80	
A3	Soot mixed with ammonium sulfate	5.86	5.43	6.20	4.83	5.98	7.86	
A2	Fresh soot – size 2	5.63	5.64	6.16	4.05	3.90	7.60	3.03
	Soot with thin SOA coating	5.97	6.00	6.94	5.90	5.02	6.80	
	Soot with thick SOA coating	5.64	5.53	5.79	4.70	4.81	6.80	
A5	PM_1 ambient-like aerosol	5.00	4.87	4.23	4.06	3.96	5.96	
	Filter type	M8060	M8060	Q250F	PTFE	PTFE	Glass fiber	Q250F
	C_m	**1.39**	**1.39**	**2.14**	**1.3**	**1.3**	**2.61**	**2.14**

The b_{atn} values of the filter-based instruments were converted to the PTAAM wavelengths of 450 nm and 808 nm using the absorption Ångström exponents determined from the ratio over the two b_{abs} values measured by the PTAAM-2λ (Supplemental Table S1). The original wavelengths of the filter-based instruments are indicated in parentheses under the instrument model. The properties of the test aerosols are listed in Table S1.
[a]Since the expanded measurement uncertainty in *C* is typically 10–15%, we recommend to round the numbers to one digit after the decimal point.
[b]Certain measurements are missing due to technical issues encountered during the measurements.

were slightly lower: 6.04 ± 0.52 and 5.99 ± 0.57 at 470 nm and 880 nm, respectively. The *C* value for the AE22 Aethalometer, which uses a quartz filter tape, was similar to the other two Aethalometer models (5.92 ± 0.87 and 6.74 ± 1.03 at 370 nm and 880 nm, respectively). The lowest *C* values were obtained for the MA200 and MA350 instruments, averaging 4.49 ± 0.86 and 4.81 ± 0.77 at 470 nm and 880 nm, respectively.

Although the absolute *C* value can be calibrated using reference absorption measurements proposed in this work, its sensitivity to aerosol physical properties (particle size distribution, coating, and cross-sensitivity to scattering) is critical for achieving stable long-term measurements under ambient conditions. For the experiments with the test aerosols A1–A3, the relative standard deviation was lowest for AE33 and AE36s (8.7% and 9.6% at 470 nm and 880 nm), followed by AE22 (14.7% and 15.4% at 370 nm and 880 nm), BC-1054 (16.4% and 11.1% at 470 nm and 880 nm), and MA200/MA350 (19% and 16.1% at 470 nm and 880 nm).

C values were generally higher for smaller soot particles compared to larger ones at 470 nm for most instruments, while no significant difference was observed at 880 nm. For BC-1054, smaller soot particles caused the largest increase in C (20%), followed by AE22 (13%) and AE33/AE36s (10%), whereas MA200 and MA350 showed no dependence on soot size.

For coated small soot (size 1), *C* values generally increased (in comparison to bare soot size 1) for most instruments, particularly for thin coatings. Compared to fresh soot, thin coatings increased C by 16% (AE33/AE36s) to 26% (MA200/MA350) at 470 nm. At 880 nm, the increase was even greater, ranging from 22% (BC-1054) to 51% (MA200/MA350). BC-1054 was the only instrument where thin coating on small soot slightly decreased *C* at 470 nm. Thick coatings on small soot particles had a smaller effect on *C* values across all instruments.

Large differences between the different DUT were observed for coated soot particles at larger sizes (size 2). For AE33 and AE36s, changes in *C* compared to fresh large soot were minimal (−1% to +6%) for both wavelengths. In contrast, BC-1054 showed a decrease of 11–20% at both wavelengths, while MA200 and MA350 exhibited an increase of 20–37% at 880 nm.

For the AE33, the *C* values determined in this study at 450 nm and 808 nm for fresh (uncoated) propane soot of series 1 (GMD_{mob}: 75.3 nm; D_v of 130.0 nm) were 6.16 and 5.75, respectively, while those for fresh soot from series 2 (GMD_{mob} of 108.4 nm; D_v of 176.6 nm) were 5.52 and 5.63, respectively. These

values agree well with the C values of 6.25 and 5.27 determined by Yus-Díez et al. (2025) for diesel soot with a D_v of 177 nm using the PTAAM-2λ as a reference instrument. Likewise, in the case of the ambient-like aerosol (A5) we observed C values of 4.84 and 5.00 at 450 nm and 808 nm, respectively. The value determined at 450 nm aligns well with the average value of 4.72 measured by Yus-Díez et al. (2025) at the same wavelength at the University of Granada urban background station, while the value of 5.01 determined at 808 nm is higher than the average value of 3.90 measured in the aforementioned study. When we consider the proposed C or harmonization values found in previous ambient intercomparison studies of aethalometer versions using the M8060 or Q250F tapes, the correction values for C in Table 2 for ambient aerosol fall between 2.6–2.8.

As discussed in Yus-Díez et al. (2025) and (Drinovec et al. 2022), higher C values are observed for soot particles compared to mineral dust particles. This is related to particle size, with smaller particles leading to higher C values. As the particles become coarse ($>$ 1 µm), the C value decreases to about 2.6–3.0. Our study confirms this finding; however, we observed a more subtle trend (C value ranging between 7.1 and 4.8 at 450 nm, Table 2) since all the test aerosols were in the sub-micrometre range. Even the ambient-like aerosol which contained mineral dust particles was generated in such a way that the number-based GMD_{mob} remained below 200 nm in order to minimize sampling artifacts related to coarse particles, such as impaction losses in bent sampling lines.

Previous studies have shown that C remains constant (for fixed particle size) up to an SSA of about 0.85, but increases with increasing SSA above this threshold value, showing a strong spike at SSA >0.9 (Drinovec et al. 2022; Yus-Díez et al. 2025). In (Yus-Díez et al. 2021), however, C started to increase at SSA $>$ 0.95. The authors argued that high C and SSA values are often associated with a large fraction of mineral dust, e.g., during Saharan dust outbreaks, and low backscatter fraction values indicative of the predominance of large particles. In our study, we found that C did not increase at SSA up to about 0.95 in line with (Yus-Díez et al. 2021). Indeed, test aerosols with high SSA generated in this study were either pure ammonium sulfate particles or (internal and external) mixtures with soot with a GMD_{mob} of <150 nm. The absence of micrometre-sized particles might explain why the C values presented in Figure 6 exhibited only a weak dependence on the aerosol SSA in the tested range (i.e., up to about 0.95). Another explanation is that for internally mixed particles, the dependence of C on size and the cross-sensitivity to scattering compete with each other.

According to ACTRIS guidelines, a wavelength-independent C parameter of 2.44 is recommended for ambient measurements using the AE33 with a M8060 filter based on the MAAP as a pseudo-reference. This value is in line with past studies (Ferrero 2024). The low C values observed in past studies compared to those determined here (∼4.9 for ambient-like aerosols) are due to systematic differences between the measurements with the PTAAM-2λ and the MAAP as highlighted by Yus-Díez et al. (2025). More information is provided below (see Figure 7).

A similar picture emerges from Figure 7, where the coefficients b_{abs} measured by in-situ photoacoustic instruments, such as the PAX (870 nm), the PAS (450 nm, 880 nm) and the MSS-2 (808 nm), are compared those obtained using the PTAAM-2λ. The figure also includes the MAAP, a filter-based instrument, which is grouped together with the in-situ instruments because it corrects for the light scattering effects of the filter.

The PAX agreed very well (typically within ∼20%) with the PTAAM-2λ when tested with fresh and aged soot, but deviated by a factor of about 1.6 when tested with ambient-like aerosols (open black squares in 7d). This behavior cannot be attributed to the aerosol SSA. As shown in panel d, the PAX agreed very well with the PTAAM-2λ for soot coated with SOM at SSA = 0.53, but its response suddenly increased by 60% when measuring ambient-like aerosols at similar SSA. This effect might be due to the presence of dust particles in test aerosol A5, but such a hypothesis would need to be further investigated in the future with dedicated experiments. It should also be highlighted that all measurements were performed at moderate to low BC concentrations (below 10 μg m^{-3}), which are environmentally relevant for most parts of Europe. Measurements at higher concentrations have been reported in Kalbermatter et al. (2022). According to Corbin et al. (2020), the excellent correlation between the eBC and EC mass concentrations measured by the PAX and CERM (centrifugal particle mass analyzer (CPMA)–electrometer reference mass system), respectively, confirms the extrapolation of the PAX calibration from approximately 4000 µg m^{-3} down to approximately 5 µg m^{-3}. Below 5 µg m^{-3}, the correlation breaks down. Considering that 10 μg m^{-3} at 870 nm correspond to an absorption of 47 Mm^{-1} and that the PAX and PAS signals were below 47 Mm^{-1} for all test points (see Figure S2), it is clear that the

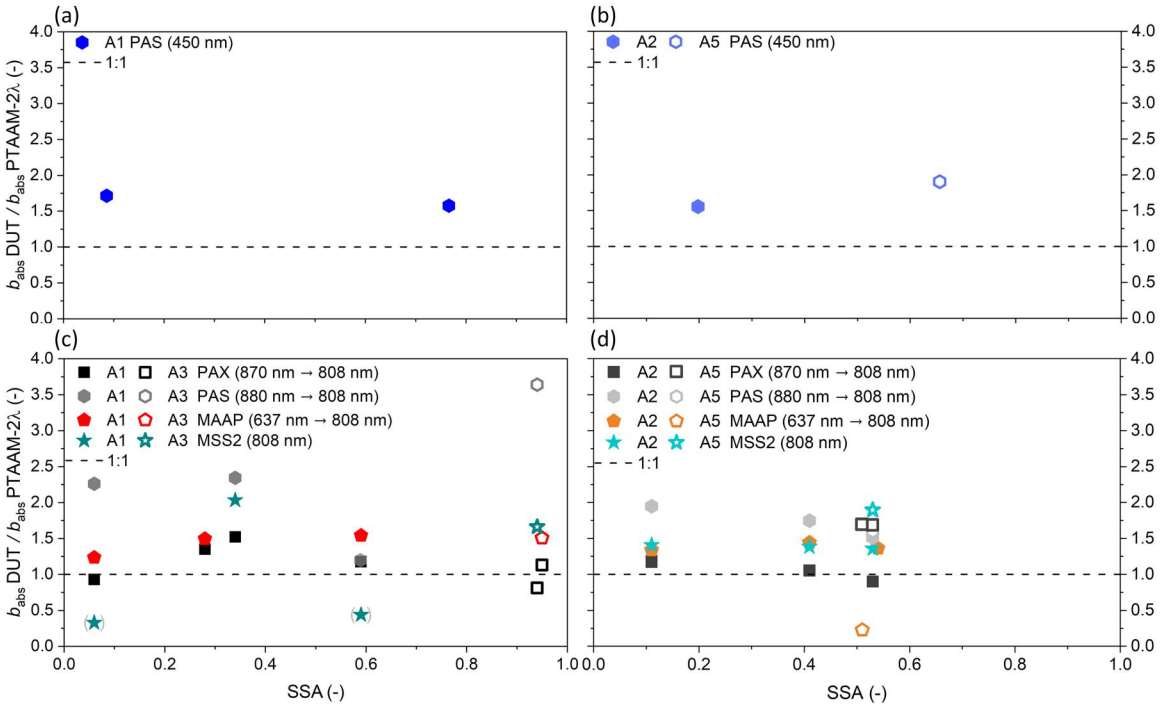

Figure 7. Ratio of b_{abs} reported by in-situ BC-measuring instruments and MAAP to the reference b_{abs} values reported by the PTAAM-2λ as a function of the aerosol SSA at (a–b) 450 nm and (c–d) 808 nm. The SSA was determined using the b_{abs} from PTAAM-2λ and the b_{scat} from the nephelometer. A1-A5 designate the test aerosols according to Table 1. The wavelength of the measurements is indicated in the legend. All b_{abs} values have been converted to a wavelength of 450 nm or 808 nm using the absorption Ångström exponents determined from the fit over the two b_{abs} values from the PTAAM-2λ (Supplemental Table S1). The dashed horizontal line represents the 1:1 instrument response to guide the eye. Data points in parentheses designate measurements out of the measurement range of the MSS-2 instrument, i.e., below 1 µg BC/m^3. Aerosol A4 consisted of highly scattering ammonium sulfate particles and is thus not included in this comparison. The data shown in parentheses were measured at concentrations below the b_{abs} limit of the instrument and should thus be disregarded.

measurements were very close to the limit of detection. This is likely one of the reasons why the deviations between PAX and PTAAM-2λ are higher than in previous studies (Kalbermatter et al. 2022).

The MAAP agreed very well with the PTAAM-2λ for fresh soot but overestimated b_{abs} by up to 50% in all other cases, in accordance with the findings of Kalbermatter et al. (2022). This is also in agreement with the factor of 1.5 reported by (Yus-Díez et al. (2025), see Figure 6a) for ambient aerosol with SSA < 0.9. In our study, in the case of ambient-like aerosols (open orange diamonds in panel d), the MAAP underestimated b_{abs} by about 70%. The reason for this behavior is not clear, especially since the MAAP overestimated b_{abs} in the case of soot mixed with ammonium sulfate (open red diamonds in panel c) which had a higher aerosol SSA of about 0.95.

The MSS-2 photoacoustic instrument, though optimized for engine emission control, showed a reasonable agreement, overestimating b_{abs} by a factor of 1.3 to 2 (cyan stars) when compared with the PTAAM-2λ. The data shown in parentheses were measured at concentrations below the b_{abs} limit of the instrument and should thus be disregarded.

The prototype photoacoustic sensor PAS-2λ overestimated b_{abs} by a factor of 1.5–1.9 in the near UV wavelength and by up to about 2.3 in the near IR region. The response PAS-2λ was very consistent, with the exception of the measurement at SSA = 0.95 in panel c. The reason for this sudden deviation is not clear. As this instrument is still under development, further investigation is needed.

Overall, the following measurement uncertainties need to be taken into account when calibrating a device-under-test (DUT), whether filter-based on *in situ* measuring instrument, against the PTAAM-2λ in terms of aerosol light absorption:

1. Measurement uncertainty of the PTAAM according to SI Table S3
2. Statistical uncertainties of the DUT (typically $\leq$4% for $k = 2$)
3. Uncertainty in the determination of AAE (in case the b_{abs} values reported by the DUT need to be

converted to one of the two wavelengths of the PTAAM).

In our study, the expanded uncertainty of the calibration factor $b_{abs,\ DUT}/b_{abs,\ PTAAM}$ lies typically below 15% ($k = 2$; 95% confidence interval). Additional wavelength-dependent measurement uncertainties may occur depending on how the end users of the filter-based photometers perform the filter-loading correction.

4. Conclusions

Series of test aerosols were produced, such as fresh soot and aged soot (i.e., coated with secondary organic material), ammonium sulfate particles, soot internally and externally mixed with ammonium sulfate and ambient-like aerosols covering a wide range of particle sizes (75–160 nm), EC/TC mass fractions (0–99%) and optical properties (SSA from almost 0 to about 1). These test aerosols simulate predominantly fresh urban aerosols, and cannot account for regional background sites. Two reference methods for the aerosol light absorption coefficient, EMS (indirect) and PTI (direct), as well as several filter-based absorption photometers and *in situ* measuring instruments were compared in the laboratory using these aerosols.

The reference measurements did not agree within their measurement uncertainties. In the blue/visible range, the EMS method overestimated the absorption coefficient of bare and aged soot by 25% and 200%, respectively. Although the deviation between EMS (CAPS PMex, DMT, USA and Aurora 4000 nephelometer, ACOEM, France) and PTI (PTAAM-2λ, Haze Instruments, Slovenia) was positive and typically increased with increasing SSA, for purely scattering aerosols (SSA >0.9) the EMS method measured 20% lower than PTI. Therefore, PTI can be used as a reference method in the entire SSA range, whereas EMS is recommended to be used as a reference method for aerosols with low to moderate (e.g., <0.6) SSA in the near-UV/visible range.

In general, the filter-based photometers that do not correct for light scattering effects reported b_{atn} values larger than the reference b_{abs} measurements with PTI by a factor of 4–9 depending on the instrument model and filter tape. In accordance with past studies, lower C values were observed for ambient-like test aerosols than for fresh soot. The derived C multiple-scattering correction factors did not show, however, a strong dependence on the aerosol SSA as the test aerosols did not contain any coarse particles. In-situ-measuring instruments and the MAAP, which corrects for light scattering effects, showed a much better agreement with PTI (typically within 50%) and can be used as a secondary or transfer standard for aerosol light absorption measurements once calibrated against the PTI reference method.

Based on the procedure described in this work, calibration factors can be determined in the laboratory under controlled and reproducible conditions by dividing b_{atn} or b_{abs} of the devices-under-test by the reference value of the PTAAM-2λ. The procedure can be easily standardized and applied to any type of filter-based absorption photometer. The setup for the generation of soot and ammonium sulfate aerosols consists of commercially available aerosol generators and is relatively affordable, whereas the generation of ambient-like aerosol requires custom-made facilities and skilled staff. A limitation of this study is that – for technical reasons related to sampling artifacts – only test aerosols in the sub-micrometre range were used for instrument comparison, thus effects related to coarse particles in ambient air combined with a high aerosol SSA could not be reproduced in the laboratory. Still, our study highlights the need for instrument calibration against reference methods, such as PTI and EMS, and provides useful recommendations on the applicability range of each reference method. Further work will focus on the development and validation of a transfer standard for field calibration of filter-based absorption photometers.

Author contributions

CRediT: **Tobias Hammer**: Data curation, Formal analysis, Investigation, Visualization; **Luka Drinovec**: Data curation, Formal analysis, Investigation, Methodology, Writing – review & editing; **Griša Močnik**: Conceptualization, Data curation, Formal analysis, Funding acquisition, Investigation, Methodology, Writing – review & editing; **Asta Gregorič**: Data curation, Formal analysis, Writing – review & editing; **Martin Rigler**: Data curation, Writing – review & editing; **Thomas Müller**: Data curation, Writing – review & editing; **Sebastian Düsing**: Data curation; **Jorge Saturno**: Project administration, Writing – review & editing; **Andreas Nowak**: Writing – review & editing; **John Backman**: Data curation, Investigation, Writing – review & editing; **Eija Asmi**: Data curation, Writing – review & editing; **Krzysztof Ciupek**: Data curation, Writing – review & editing; **Douglas Walker**: Data curation; **Maria Gini**: Data curation, Writing – review & editing; **Konstantinos Eleftheriadis**: Supervision, Writing – review & editing; **Stergios Vratolis**: Data curation; **Jeffrey Blair**: Data curation; **Ivan Iskra**: Data curation; **Kyan Shlipak**: Data curation; **Weidong Chen**: Data curation, Investigation, Writing – review & editing; **Goufrane Abichou**: Data curation; **Yongyong Hu**: Data curation; **Jošt V. Lavrič**: Data curation,

Investigation; **Johannes Murg**: Data curation, Writing – review & editing; **Michael Arndt**: Data curation; **Alejandro Keller**: Writing – review & editing; **Ernest Weingartner**: Writing – review & editing; **Konstantina Vasilatou**: Conceptualization, Funding acquisition, Methodology, Project administration, Writing – original draft.

Disclosure statement

Luka Drinovec and Griša Močnik are affiliated with Haze Instruments d.o.o., Asta Gregorič and Martin Riegler with Aerosol d.o.o., Jeffrey Blair, Ivan Iskra and Kyan Shlipak with AethLabs, Jošt Lavrič with ACOEM, Johannes Murg and Michael Arndt with AVL.

Funding

This research has received funding by the European Partnership in Metrology [Research grant 22NRT02 StanBC], co-financed from the European Union's Horizon Europe Research and Innovation Programme and by the Participating State. Views and opinions expressed are however those of the authors only and do not necessarily reflect those of the European Union or EURAMET. Neither the European Union nor the granting authority can be held responsible for them. GM acknowledges support from the Slovenian Research Agency program P1-0385 and projects L2-4485 and V1-2373. KV acknowledges support from the Swiss State Secretariat for Education, Research and Innovation [Contract Nr. 23.00435].

ORCID

Jorge Saturno http://orcid.org/0000-0002-3761-3957
Andreas Nowak http://orcid.org/0000-0002-3773-1726
Jošt V. Lavrič http://orcid.org/0000-0003-3610-9078

References

Anderson TL et al. 1996. Performance characteristics of a high-sensitivity, three-wavelength, total scatter/backscatter nephelometer. J Atmos Oceanic Technol. 13(5):967–986. https://doi.org/10.1175/1520-0426(1996)013<0967:PCOAHS>2.0.CO;2

Arnott WP, Moosmüller H, Walker JW. 2000. Nitrogen dioxide and kerosene-flame soot calibration of photoacoustic instruments for measurement of light absorption by aerosols. Rev Sci Instrum. 71(12):4545–4552. https://doi.org/10.1063/1.1322585

Backman J et al. 2017. On Aethalometer measurement uncertainties and an instrument correction factor for the Arctic. Atmos Meas Tech. 10(12):5039–5062. https://doi.org/10.5194/amt-10-5039-2017

Bluvshtein N et al. 2017. Calibration of a multi-pass photoacoustic spectrometer cell using light-absorbing aerosols. Atmos Meas Tech. 10(3):1203–1213. https://doi.org/10.5194/amt-10-1203-2017

Cavalli F, Viana M, Yttri KE, Genberg J, Putaud J-P. 2010. Toward a standardised thermal-optical protocol for measuring atmospheric organic and elemental carbon: the EUSAAR protocol. Atmos Meas Tech. 3(1):79–89. https://doi.org/10.5194/amt-3-79-2010

Corbin JC et al. 2020. Closure between particulate matter concentrations measured ex situ by thermal – optical analysis and in situ by the CPMA – electrometer reference mass system. Aerosol Sci Technol. 54(11):1293–1309. https://doi.org/10.1080/02786826.2020.1788710

Corbin JC, Moallemi A, Poitras D, Sipkens TA, Oliaee JN. 2025. Self-calibrating aerosol absorption measurements using co-located TDLAS and tunable-wavelength photothermal interferometry. Aerosol Sci Technol. 59(7):877–891. https://doi.org/10.1080/02786826.2025.2469780

Cremer JW, Covert PA, Parmentier EA, Signorell R. 2017. Direct measurement of photoacoustic signal sensitivity to aerosol particle size. J Phys Chem Lett. 8(14):3398–3403. https://doi.org/10.1021/acs.jpclett.7b01288

Davies NW et al. 2018. On the accuracy of aerosol photoacoustic spectrometer calibrations using absorption by ozone. Atmos Meas Tech. 11(4):2313–2324. https://doi.org/10.5194/amt-11-2313-2018

Devi A, Satheesh SK. 2022. Global maps of aerosol single scattering albedo using combined CERES-MODIS retrieval. Atmos Chem Phys. 22(8):5365–5376. https://doi.org/10.5194/acp-22-5365-2022

Drinovec L et al. 2022. A dual-wavelength photothermal aerosol absorption monitor: design, calibration and performance. Atmos Meas Tech. 15(12):3805–3825. https://doi.org/10.5194/amt-15-3805-2022

Ess MN et al. 2021. Optical and morphological properties of soot particles generated by the miniCAST 5201 BC generator. Aerosol Sci Technol. 55(7):828–847. https://doi.org/10.1080/02786826.2021.1901847

Ess MN, Bertò M, Keller A, Gysel-Beer M, Vasilatou K. 2021. Coated soot particles with tunable, well-controlled properties generated in the laboratory with a miniCAST BC and a micro smog chamber. J Aerosol Sci. 157(May):105820. https://doi.org/10.1016/j.jaerosci.2021.105820

Ess MN, Vasilatou K. 2019. Characterization of a new miniCAST with diffusion flame and premixed flame options: generation of particles with high EC content in the size range 30 nm to 200 nm. Aerosol Sci Technol. 53(1):29–44. https://doi.org/10.1080/02786826.2018.1536818

European Parliament. 2024. Directive (EU) 2024/2881 of the European Parliament and of the Council of 23 October 2024 on ambient air quality and cleaner air for Europe. https://eur-lex.europa.eu/legal-content/EN/TXT/?uri=OJ:L_202402881

Foster K, Pokhrel R, Burkhart M, Murphy S. 2019. A novel approach to calibrating a photoacoustic absorption spectrometer using polydisperse absorbing aerosol. Atmos Meas Tech. 12(6):3351–3363. https://doi.org/10.5194/amt-12-3351-2019

Ganguly D, Jayaraman A, Rajesh TA, Gadhavi H. 2006. Wintertime aerosol properties during foggy and nonfoggy days over urban center Delhi and their implications for shortwave radiative forcing. J Geophys Res. 111(D15):D15217. https://doi.org/10.1029/2005JD007029

Haywood JM, Shine KP. 1995. The effect of anthropogenic sulfate and soot aerosol on the clear sky planetary radiation budget. Geophys Res Lett. 22(5):603–606. https://doi.org/10.1029/95GL00075

Horender S et al. 2021. Facility for production of ambient-like model aerosols (PALMA) in the laboratory: application in the intercomparison of automated PM monitors with the reference gravimetric method. Atmos Meas Tech. 14(2):1225–1238. https://doi.org/10.5194/amt-14-1225-2021

Horender S, Tancev G, Auderset K, Vasilatou K. 2021. Traceable PM2.5 and PM10 calibration of low-cost sensors with ambient-like aerosols generated in the laboratory. Appl Sci. 11(19):9014. https://doi.org/10.3390/app11199014

Kalbermatter DM et al. 2022. Comparing black-carbon- and aerosol-absorption-measuring instruments – a new system using lab-generated soot coated with controlled amounts of secondary organic matter. Atmos Meas Tech. 15(2):561–572. https://doi.org/10.5194/amt-15-561-2022

Keller A, Burtscher H. 2012. A continuous photo-oxidation flow reactor for a defined measurement of the SOA formation potential of wood burning emissions. J Aerosol Sci. 49(12):9–20. https://doi.org/10.1016/j.jaerosci.2012.02.007

Keller A et al. 2022. The Organic Coating Unit, an all-in-one system for reproducible generation of secondary organic matter aerosol. Aerosol Sci Technol. 56(10):947–958. https://doi.org/10.1080/02786826.2022.2110448

Keller A, Specht P, Steigmeier P, Weingartner E. 2023. A novel measurement system for unattended, in situ characterization of carbonaceous aerosols. Aerosol Res. 1(1):65–79. https://doi.org/10.5194/ar-1-65-2023

Koch D, Del Genio AD. 2010. Black carbon semi-direct effects on cloud cover: review and synthesis. Atmos Chem Phys. 10(16):7685–7696. https://doi.org/10.5194/acp-10-7685-2010

Lack DA, Lovejoy ER, Baynard T, Pettersson A, Ravishankara AR. 2006. Aerosol absorption measurement using photoacoustic spectroscopy: sensitivity, calibration, and uncertainty developments. Aerosol Sci Technol. 40(9):697–708. https://doi.org/10.1080/02786820600803917

Leni Z et al. 2022. Role of secondary organic matter on soot particle toxicity in reconstituted human bronchial epithelia exposed at the air-liquid interface. Environ Sci Technol. 56(23):17007–17017. https://doi.org/10.1021/acs.est.2c03692

Massoli P et al. 2009. Uncertainty in light scattering measurements by TSI nephelometer: results from laboratory studies and implications for ambient measurements. Aerosol Sci Technol. 43(11):1064–1074. https://doi.org/10.1080/02786820903156542

Mehri R, Sipkens TA, Smallwood GJ, Johnson M, Corbin JC. 2025. Size-resolved measurements of the light absorption properties of soot aerosols from a gas turbine engine. Appl Phys B. 131(5):1–10. https://doi.org/10.1007/s00340-025-08459-2

Modini RL et al. 2021. Detailed characterization of the CAPS single-scattering albedo monitor (CAPS PMssa) as a field-deployable instrument for measuring aerosol light absorption with the extinction-minus-scattering method. Atmos Meas Tech. 14(2):819–851. https://doi.org/10.5194/amt-14-819-2021

Moteki N et al. 2010. Radiative transfer modeling of filter-based measurements of light absorption by particles: importance of particle size dependent penetration depth. J Aerosol Sci. 41(4):401–412. https://doi.org/10.1016/j.jaerosci.2010.02.002

Müller T, Fiebig M. 2018. ACTRIS In Situ Aerosol: guidelines for Manual QC of AE33 absorption photometer data. Retrieved from https://www.actris-ecac.eu/

Müller T et al. 2011. Characterization and intercomparison of aerosol absorption photometers: result of two intercomparison workshops. Atmos Meas Tech. 4(2):245–268. https://doi.org/10.5194/amt-4-245-2011

Müller T, Laborde M, Kassell G, Wiedensohler A. 2011. Design and performance of a three-wavelength LED-based total scatter and backscatter integrating nephelometer. Atmos Meas Tech. 4(6):1291–1303. https://doi.org/10.5194/amt-4-1291-2011

Nakayama T et al. 2010. Size-dependent correction factors for absorption measurements using filter-based photometers: PSAP and COSMOS. J Aerosol Sci. 41(4):333–343. https://doi.org/10.1016/j.jaerosci.2010.01.004

Nakayama T et al. 2015. Characterization of a three wavelength photoacoustic soot spectrometer (PASS-3) and a photoacoustic extinctiometer (PAX). J Meteorol Soc Jpn. 93(2):285–308. https://doi.org/10.2151/jmsj.2015-016

Niranjan R, Thakur AK. 2017. The toxicological mechanisms of environmental soot (black carbon) and carbon black: focus on Oxidative stress and inflammatory pathways. Front Immunol. 8(JUN):763. https://doi.org/10.3389/fimmu.2017.00763

Onasch TB et al. 2015. Single scattering albedo monitor for airborne particulates. Aerosol Sci Technol. 49(4):267–279. https://doi.org/10.1080/02786826.2015.1022248

Petzold A, Onasch T, Kebabian P, Freedman A. 2013. Intercomparison of a Cavity Attenuated Phase Shift-based extinction monitor (CAPS PMex) with an integrating nephelometer and a filter-based absorption monitor. Atmos Meas Tech. 6(5):1141–1151. https://doi.org/10.5194/amt-6-1141-2013

Renzi L et al. 2025. The role of size in the multiple scattering correction C for dual-spot aethalometer: a field and laboratory investigation. Atmos Meas Tech. 19:1365–1383. https://egusphere.copernicus.org/preprints/2025/egusphere-2025-2823/

Salo L et al. 2024. Black carbon instrument responses to laboratory generated particles. Atmos Pollut Res. 15(5):102088. https://doi.org/10.1016/j.apr.2024.102088

Savadkoohi M et al. 2024. Recommendations for reporting equivalent black carbon (eBC) mass concentrations based on long-term pan-European in-situ observations. Environ Int. 185:108553. https://doi.org/10.1016/j.envint.2024.108553

Sedlacek AJ. 2006. Real-time detection of ambient aerosols using photothermal interferometry: folded Jamin interferometer. Rev Sci Instrum. 77(6):064903. https://doi.org/10.1063/1.2205623

Sharma N, Arnold IJ, Moosmüller H, Arnott WP, Mazzoleni C. 2013. Photoacoustic and nephelometric spectroscopy of aerosol optical properties with a supercontinuum light source. Atmos Meas Tech. 6(12):3501–3513. https://doi.org/10.5194/amt-6-3501-2013

Singh S, Fiddler MN, Smith D, Bililign S. 2014. Error analysis and uncertainty in the determination of aerosol optical properties using cavity ring-down spectroscopy, integrating nephelometry, and the extinction-minus-

scattering method. Aerosol Sci Technol. 48(12):1345–1359. https://doi.org/10.1080/02786826.2014.984062

Wang Y et al. 2017. Fractal dimensions and mixing structures of soot particles during atmospheric processing. Environ Sci Technol Lett. 4(11):487–493. https://doi.org/10.1021/acs.estlett.7b00418

Yuan J et al. 2021. Variability in the mass absorption cross section of black carbon (BC) aerosols is driven by BC internal mixing state at a central European background site (Melpitz, Germany) in winter. Atmos Chem Phys. 21(2):635–655. https://doi.org/10.5194/acp-21-635-2021

Yus-Díez J et al. 2021. Determination of the multiple-scattering correction factor and its cross-sensitivity to scattering and wavelength dependence for different AE33 Aethalometer filter tapes: a multi-instrumental approach. Atmos Meas Tech. 14(10):6335–6355. https://doi.org/10.5194/amt-2021-46

Yus-Díez J et al. 2025. Characterization of filter photometer artefacts in soot and dust measurements – laboratory and ambient experiments using a traceably-calibrated aerosol absorption reference. Atmos Meas Tech. 18(13):3073–3093. https://doi.org/10.5194/amt-18-3073-2025

Zhao W et al. 2021. Determination of equivalent black carbon mass concentration from aerosol light absorption using variable mass absorption cross section. Atmos Meas Tech. 14(2):1319–1331. https://doi.org/10.5194/amt-14-1319-2021